Title

CH4 sources estimated from atmospheric observations of CH4 and its C-13/C-12 isotopic ratios: 1. Inverse modeling of source processes

Journal

Global Biogeochemical Cycles, 18(4)

ISSN

0886-6236

Authors

Mikaloff Fletcher, S.E.
Tans, P P
Bruhwiler, L M
et al.

Publication Date

2004-10-01

Peer reviewed

CH_4 sources estimated from atmospheric observations of CH_4 and its $^{13}C/^{12}C$ isotopic ratios: 1. Inverse modeling of source processes

Sara E. Mikaloff Fletcher[1]
Cooperative Institute for Research in Environmental Science (CIRES), University of Colorado, Boulder, Colorado, USA

Pieter P. Tans, Lori M. Bruhwiler, and John B. Miller
National Oceanic and Atmospheric Administration Climate Modeling Diagnostics Laboratory (NOAA CMDL), Boulder, Colorado, USA

Martin Heimann
Max-Planck-Institut für Biogeochemie, Jena, Germany

Received 14 January 2004; revised 13 June 2004; accepted 20 June 2004; published XX Month 2004.

[1] A time-dependent inverse modeling approach that estimates the global magnitude of atmospheric methane sources from the observed spatiotemporal distribution of atmospheric CH_4, $^{13}C/^{12}C$ isotopicratios, and a priori estimates of the source strengths is presented. Relative to the a priori source estimates, the inverse model calls for increased CH_4 flux from sources with strong spatial footprints in the tropics and Southern Hemisphere and decreases in sources in the Northern Hemisphere. The CH_4 and $^{13}C/^{12}C$ isotopic ratio observations suggest an unusually high CH_4 flux from swamps ($\sim$200 ± 44 Tg CH_4/yr) and biomass burning (88 ± 18 Tg CH_4/yr) with relatively low estimates of emissions from bogs ($\sim$20 ± 14 Tg CH_4/yr), and landfills (35 ± 14 Tg CH_4/yr). The model results support the hypothesis that the 1998 CH_4 growth rate anomaly was caused in part by a large increase in CH_4 production from wetlands, and indicate that wetland sources were about 40 Tg CH_4/yr higher in 1998 than 1999. *INDEX TERMS:* 0315 Atmospheric Composition and Structure: Biosphere/atmosphere interactions; 0322 Atmospheric Composition and Structure: Constituent sources and sinks; 0368 Atmospheric Composition and Structure: Troposphere—constituent transport and chemistry; 1040 Geochemistry: Isotopic composition/chemistry; *KEYWORDS:* inverse model, isotopic signature, methane

Citation: Mikaloff Fletcher, S. E., P. P. Tans, L. M. Bruhwiler, J. B. Miller, and M. Heimann (2004), CH_4 sources estimated from atmospheric observations of CH_4 and its $^{13}C/^{12}C$ isotopic ratios: 1. Inverse modeling of source processes, *Global Biogeochem. Cycles*, *18*, GBXXXX, doi:10.1029/2004GB002223.

1. Introduction

[2] High-quality, quantitative estimates of the CH_4 budget are crucial to predicting climate change, managing Earth's carbon reservoirs, and understanding atmospheric chemistry. CH_4 is the second most important greenhouse gas after CO_2 and is responsible for approximately 20% of the direct radiative forcing from all long-lived greenhouse gases [*Intergovernmental Panel on Climate Change* (*IPCC*), 2001]. CH_4 is the second most important sink for OH radical, which is the primary determinant of the oxidizing capacity of Earth's atmosphere. In addition, CH_4 plays an important role in tropospheric O3 pollution [*Fiore et al.*, 2002], and about half of all stratospheric water vapor comes from the oxidation of CH_4 [*Jones and Pyle*, 1984].

[3] Over the last 150 years, the mixing ratio of CH_4 in the atmosphere has more than doubled [*Etheridge et al.*, 1998], primarily as the result of the addition of anthropogenic methane sources such as ruminant animal husbandry and rice agriculture, production of natural gas, coal mining, biomass burning, and landfills. CH_4 is also produced naturally by anaerobic bacteria in wetlands, dry tundra, and termites. The oceans evolve CH_4 from anaerobic bacteria in surface waters, fossil methane in marine sediments, and destabilization of methane hydrates, although these sources are thought to be relatively small due to oxidation of CH_4 in the water column. Oxidation of CH_4 by OH radical in the troposphere is the principle CH_4 sink, accounting for approximately 90% of all CH_4 destruction. In addition, CH_4 is oxidized by methanotrophic bacteria in aerobic soils and by reaction with OH, Cl, and O (1D) in the stratosphere.

[4] Despite the importance of CH_4 to Earth's radiative balance and atmospheric chemistry, there are still large

[1]Now at Department of Atmospheric and Oceanic Sciences, University of California, Los Angeles, California, USA.

0886-6236/04/2004GB002223$12.00

t1.1 **Table 1.** Methane Budget and the Mean $\delta^{13}CH_4$ Isotopic Signatures of the Sources and Sinks[a]

t1.2 Sources	A Priori Estimates, Tg CH_4/yr	Range of Estimates Reported by *IPCC* [2001], Tg CH_4/yr	Mean Isotopic Signature
t1.3 Total wetlands		92–237	−58‰[i]
t1.4 Swamps	91[a]		
t1.5 Bogs and tundra	54[a]		
t1.6 Rice agriculture	60[b]	25–100	−63‰[i]
t1.7 Ruminant animals	93[b]	80–115	−60‰[i]
t1.8 Termites	20[c]	20–20	−70‰[i]
t1.9 Biomass burning	52[d]	23–55	−25‰[i]
t1.10 Energy		75–109	
t1.11 Coal	38[b]		−37‰[i]
t1.12 Natural gas and other industrial	57[b]		−44‰[i]
t1.13 Landfills	50[e]	35–73	−55‰[i]
t1.14 Ocean	10[f]	10–15	−60‰[i]
t1.15 Hydrates	5[f]	5–10	−60‰[i]
t1.16 **Total source**	**530**	**500–600**	**∼−53‰**[i]
t1.17 Sinks	A Priori Estimates, Tg CH_4/yr	Range of Estimates Reported by *IPCC* [2001], Tg CH_4/yr	Isotopic Fractionation
t1.18 Tropospheric OH	507[g]	450–510	5.4‰[j]
t1.19 Stratospheric loss	40[h]	40–46	12‰[k]
t1.20 Soils	30[h]	10–30	22‰[l]
t1.21 **Total**	**577**		**∼ 6.7‰**

[a]IPCC range of estimates covers the high and low estimates from a suite of budgets compiled using different approaches listed in the t1.22 *IPCC* [2001] report. These estimates are typical of the range of estimates that can be found in the literature for CH_4 sources.
t1.23 [b]*Lelieveld et al.* [1998].
t1.24 [c]EDGAR emissions database [*Olivier et al.*, 1996].
t1.25 [d]*Sanderson* [1996].
t1.26 [e]*Levine et al.* [2000].
t1.27 [f]*Bingemer and Crutzen* [1987].
t1.28 [g]*Cicerone and Oremland* [1988].
t1.29 [h]On the basis of *Spivakovsky et al.* [2000] OH fields and model CH_4 mixing ratios, tuned to *IPCC* [2001] total CH_4 loss.
t1.30 [i]*IPCC* [2001].
t1.31 [j]*Whiticar* [1993].
t1.32 [k]*Cantrell et al.* [1990].
t1.33 [l]*Brenninkmeijer et al.* [1995], reflecting the total observed isotopic fractionation due to OH, O^1D, and Cl in the stratosphere.
t1.34 [m]*Tyler et al.* [1994].

uncertainties in estimates of the CH_4 fluxes as shown by the wide range of *IPCC* [2001] estimates in Table 1, and the causes for the observed variability in the recent CH_4 growth rate are not well understood [*Dlugokencky et al.*, 2003, 2001, 1998]. The growth rate of atmospheric CH_4 for the 1990s has an overall decreasing trend and includes anomalous increases in the growth rate in 1991 and 1998 and a large decrease in the growth rate during 1992. Much progress has been made toward qualitatively attributing these features to source and sink processes by correlating them to changes in climate, fossil fuel consumption, and other phenomena [i.e., *Dlugokencky et al.*, 1996; *Bekki et al.*, 1994; *Dlugokencky et al.*, 1998]. The 1998 growth rate anomaly occurred during an unusually warm year, marked by precipitation anomalies associated with the transition from a strong El Niño condition to a La Niña [*Bell et al.*, 1999; *Curtis et al.*, 2001]. Comparisons between the CH_4 growth rate anomaly and a process-based model of wetlands which included temperature and precipitation anomalies illustrated that increased biospheric production could account for this event [*Dlugokencky et al.*, 2001]. Conversely, *Langenfelds et al.* [2002] and *Van der Werf et al.* [2004] attributed much of the 1997–1998 CH_4 anomaly to extensive fires.

[5] Process-level estimates of CH_4 fluxes have significant uncertainties due to the aggregation or extrapolation of local measurements, often representing only a limited time period, of sources with large spatial and temporal variability to regional or global scales. Model simulations of the CH_4 atmospheric mixing ratio resulting from these bottom-up source estimates typically overestimate the interhemispheric gradient of CH_4 relative to the observations [i.e., *Fung et al.*, 1991; *Hein et al.*, 1997; *Houweling et al.*, 1999] (also Figure 1, this study) implying that the sources may be overestimated in the Northern Hemisphere (NH) and/or underestimated in the Southern Hemisphere (SH).

[6] Inverse modeling is a "top-down" approach to optimize trace gas flux estimates using observations of atmospheric mixing ratios, a model of atmospheric transport, the spatial distributions of the sources, and, in most cases, a prior estimate of the source magnitudes to calculate an optimal combination of fluxes to match the observational

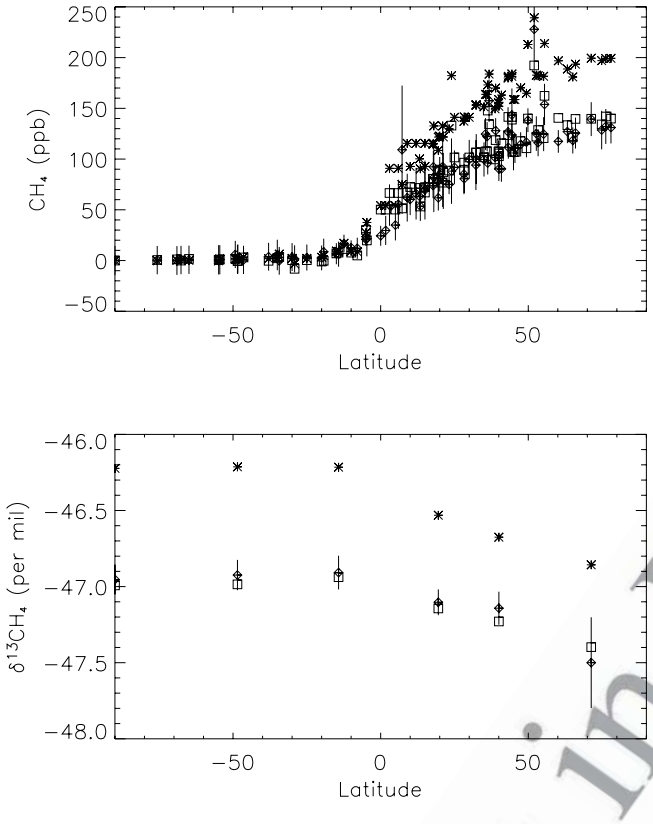

Figure 1. Latitudinal gradient of (top) CH_4 and (bottom) $\delta^{13}CH_4$ of the observations (diamonds), forward simulation based on the a priori estimates (asterisks), and forward simulation based on the a posteriori source estimates (squares). Error bars on the observations reflect the standard deviation of the individual observations from the annual mean.

data and our current understanding of the source processes. This technique has been applied to several atmospheric trace gases including CO_2 [e.g., *Enting and Mansbridge*, 1989; *Tans et al.*, 1990; *Fan et al.*, 1998; *Gurney et al.*, 2002], CH_4 [e.g., *Hein et al.*, 1997; *Houweling et al.*, 1999], and CO [e.g., *Kasibhatla et al.*, 2002; *Bergamaschi et al.*, 2000b].

[7] One of the difficulties associated with using atmospheric observations of CH_4 to gain insight into the sources and sinks of CH_4 is that atmospheric observations primarily provide information regarding the spatial distribution of the total CH_4 flux, and some of the CH_4 source processes have a great deal of spatial overlap. Two approaches have been used to address this issue in CH_4 inverse studies. In one approach, an inverse model was used to determine the spatial distribution of CH_4 flux required to match the atmospheric observations without differentiating the flux by source process [*Houweling et al.*, 1999]. While this technique was able to reduce the uncertainty of the total CH_4 flux, especially in the NH, it provided limited insight into the physical processes responsible for the differences between the inverse model and process-based estimates. In an alternate approach, inverse models have been used to estimate the magnitude of the total global fluxes for separate source process based on the spatial distribution of the sources [e.g., *Hein et al.*, 1997; *Bergamaschi et al.*, 2000a, 2001] or from separate source processes across large spatial regions [*Chen*, 2004]. These inverse estimates tend to find decreases in source estimates relative to the prior estimates for source processes with larger footprints in the NH and increases in sources with large footprints in the SH, consistent with the forward modeling results suggesting that a priori sources lead to an overestimate of the interhemispheric gradient. While *Hein et al.* [1997] were able to reduce the uncertainties associated with the source estimates using the station observations; they also found that a variety of different source scenarios could also match the observational data, in line with the earlier work of *Fung et al.* [1991].

[8] Including observations of isotopic ratios in CH_4 inversions may add a unique constraint to the problem by taking advantage of differences between the isotopic discrimination associated with different source processes. In addition to providing a new constraint to the underdetermined CH_4 inverse problem, observations of isotopic ratios may improve partitioning of the flux estimates between source processes with similar spatial patterns but differing isotopic signatures. The source processes can be separated into four broad categories based on their isotopic signatures: bacterial sources, including wetlands, rice paddies, ruminant animals, and termites, biomass burning, fossil sources, and landfills (Table 1).

[9] Previous inverse model studies have made limited use of observations of stable isotopes of CH_4. *Bergamaschi et al.* [2000a] used the NOAA/CMDL observations of CH_4 to estimate the magnitude of the CH_4 source, then used observations from two SH stations and one NH station of the $^{13}C/^{12}C$ isotopic ratio in atmospheric CH_4 and the inverse CH_4 source estimates to optimize the isotopic signature of each source process. *Hein et al.* [1997] used observation of ^{13}C from three stations to further constrain their inverse study and optimize the isotopic signatures of the sources. However, since in the latter study only stations in the NH were used, interhemispheric gradient information was not included. Using a two-box model with annual, hemispheric averages of $^{13}C/^{12}C$ and CH_4, *Miller et al.* [2002] conducted a simple inversion for two general CH_4 source categories, bacterial CH_4 production and biomass burning, holding fossil fuel sources fixed. These studies found that measurements of $^{13}C/^{12}C$ isotopic ratios combined with measurements of CH_4 could provide constraints to the methane budget.

[10] Here we present the first time-dependent inverse estimates of CH_4 constrained by both the GLOBALVIEW-CH_4 data product and observations of the $^{13}C/^{12}C$ isotopic ratios from six NOAA/CMDL stations from 1998–1999. The variations between the two inverse model years are shown and discussed in the context of the 1998 methane growth rate anomaly, and the inverse estimates are compared with recent process-based estimates and discussed in the context of observed physical phenomena likely to affect the source processes. In addition, the sensitivity of the inverse estimates is tested in response to

several potential sources of error. In a companion paper [*Mikaloff Fletcher et al.*, 2004], a complimentary technique will be used to interpret the relative source process contributions to regional CH_4 inverse estimates with observations of $^{13}C/^{12}C$ isotopic ratios in CH_4.

2. Methods

[11] This study employs a time dependent assimilation and source retrieval technique [*Bruhwiler et al.*, 2000]. It is a conceptually straightforward mass balance approach that has minimal dependence on prior estimates. The behavior of a trace gas over time in the presence of sources, sinks, and transport processes can be described by the mass continuity equation,

$$\frac{dy}{dt} = \mathbf{T} \bullet y + S, \tag{1}$$

where $\mathbf{T}$ is an operator that describes the atmospheric transport processes, y is the atmospheric abundance of the trace gas, and S is the net effect of sources and sinks.

[12] The effect of the sources over a given time step from a defined source region on the atmospheric abundance of a trace gas at an observing station in the absence of transport error over a given time period can be described by

$$y_j^{\text{obs}} - y_j = \sum_{i=1,\text{nsrc}} \mathbf{H}_{i,j} x_i. \tag{2}$$

In this equation, y^{obs} is the observed mixing ratio at station j, x_i is the source strength for the ith source region, and nsrc is the total number of source regions. The theoretical mixing ratio in the absence of sources, y, is calculated by applying the transport model to the three dimensional trace gas distribution from the previous time step without including source processes. $\mathbf{H_i}$ is the basis function matrix which describes the signal observed at the station after one time step in response to an arbitrary, steady source from the ith source region, calculated by emitting 1 Tg CH_4/yr from the source region and allowing the transport model to act on these emissions. After the emissions have been transported for one inversion time step, in this case 1 month, the resulting mixing ratio distribution is sampled at the station locations. Thus, in the absence of error, the difference between the observed mixing ratio of a trace gas and the modeled mixing ratio in the absence of sources is described as a linear combination of the sources. This calculation was done monthly over the period of the inversion, 1998–2000. One important limitation to our inversion is that the basis functions only reflect 1 month of model transport. Errors in the flux estimates for a given month step are propagated to the next time step because they influence the modeled spatial distribution of the trace gas, y_j, in equation (2). Therefore an underestimate in the flux from a region in a given month may lead to an underestimate in the flux from that region or a neighboring region in a later month, since no mechanism is included for flux estimates from previous months to be adjusted based on observations for the current month. This is likely to result in increased temporal noise in the inverse estimates.

[13] In addition to the station observation constraints used in the *Bruhwiler et al.* [2000], constraints from process-based estimates of the sources, or a priori estimates, have been included. A Singular Value Decomposition (SVD) is applied to determine the optimal source magnitudes required to match the observations and the prior estimates. When including a priori estimates, the relative weighting of the atmospheric observations and the a priori estimates based on their estimated uncertainty, σ, plays a critical role in the inverse flux estimates. In the limit of high model-data mismatch error relative to the prior uncertainty, the a posteriori inverse estimates may primarily reflect the a priori estimates. In this inversion, the uncertainty associated with the prior estimates was set equal to the difference between the high and low estimates for each source process published in the *IPCC* [2001] (Table 1), except in the case of termites, where the uncertainty was assumed to be 20 Tg CH_4/yr. The uncertainty associated with the observational data is much less straightforward, because it is not primarily associated with the measurements themselves; rather, it due to limitations in the model's ability to describe the station observations. In this study, an average uncertainty was estimated for both continental and coastal or marine sites based on the mean standard deviation of the residuals from the smooth curve in the observations. Sites sampling marine air were assigned a model-data mismatch uncertainty of 10 ppb and those sampling continental air were assigned an uncertainty of 21 ppb. This choice of sigma values results in a primarily data-driven inversion with the a priori constraints only ruling out truly nonphysical results such as uptake due to processes known to act exclusively as sources.

[14] In this experiment, following *Hein et al.* [1997], each source process is estimated separately with the spatial distribution of the source processes represented by the NASA Goddard Institute for Space Studies (GISS) flux maps described by *Fung et al.* [1991]. As in the work of Fung et al., the five major wetland types [*Matthews and Fung*, 1987] are grouped into two broad categories: bogs, which occur mainly between 50°N and 70°N, and swamps, which primarily occur in the tropics. The isotopic signature of each source is prescribed in order to use the isotopic ratios measured at each observing station as additional constraints on the methane flux estimates. It is important to note that source process inversions are subject to significant error due to the inherent assumption that the a priori spatial distribution of each source process is correct and has little or no interannual variability. In addition, the large spatial extent of the source processes may lead to errors. Since the internal spatial distribution of the sources for a model region cannot be adjusted by the inversion and the sampling network is sparse, inaccuracies and unrepresented variability in the spatial pattern for the region have been shown to introduce biases, also called ''aggregation error'' [*Kaminski et al.*, 1999]. Conversely, if very small model regions are used in an inverse model, the current observing network is unlikely to be able to provide sufficient constraints for many of the model regions, resulting in

inverse estimates that are strongly determined by a priori estimates.

[15] Equation (2) can be rewritten in terms of ^{13}C as

$$R_j^{\mathrm{obs}} y_j^{\mathrm{obs}} - R_j y_j = \sum_{i=1,\mathrm{nsrc}} \mathbf{H}_{i,j} R_i x_i, \tag{3}$$

where R_j^{obs} and R_j represent the $^{13}C/^{12}C$ ratios of the observations and the model simulation, calculated in the absence of sources during the time step, and R_i is the isotopic ratio of $^{13}C/^{12}C$ in CH_4 observed for each source process. In order to isolate very small changes in the isotopic ratio due to the isotope effects of source and sink processes, stable isotope ratios are conventionally expressed as $\delta^{13}C$, the fractional deviation of the isotopic ratio of the sample, R_{sample}, from a standard, $R_{\mathrm{reference}}$.

$$\delta^{13}C = \left(\frac{R_{\mathrm{sample}}}{R_{\mathrm{reference}}} - 1\right) \times 1000. \tag{4}$$

By using a linear combination of equation (2) and equation (3) and applying the definitions of $\delta^{13}C$ (equation (4)), we can write an equation for the CH_4 sources in terms of both $\delta^{13}CH_4$ and CH_4 (Appendix A).

$$\delta_j^{\mathrm{obs}} y_j^{\mathrm{obs}} - \delta_j y_j = \sum_{i=1,\mathrm{nr}} \mathbf{H}_{i,j} x_i \delta_i^{\mathrm{src}}, \tag{5}$$

where δ_i^{src} is the isotopic signature of the ith source process. The uncertainty estimate, equation (5), which plays an important role in estimating the a posteriori error estimates and the relative weighting of each linear equation in the system of linear equations, is expressed in terms of the uncertainty associated with δ, σ_j^{δ}, and the uncertainty associated with y, σ_j^{δ}.

$$\sigma = \sqrt{\left(\sigma_j^{\delta} y_j\right)^2 + \left(\delta_j \sigma_j^{y}\right)^2}. \tag{6}$$

Thus, if equation (5) were used, the uncertainty for the isotopic signature constraints would be strongly dependent on the arbitrary reference value selected in equation (4), $R_{\mathrm{reference}}$. Therefore we set the reference ratio equal to the calculated isotopic ratio expected in the absence of sources, which is different for each station, such that the calculated $\delta \equiv 0$ and equation (5) reduces to

$$\delta_j^{*\mathrm{obs}} y_j^{\mathrm{obs}} = \sum_{i=1,\mathrm{nr}} \mathbf{H}_{i,j} x_i \delta_i^{*\mathrm{src}}, \tag{7}$$

where $\delta^{*\mathrm{obs}}$ and $\delta_i^{*\mathrm{src}}$ represent the delta values defined in terms of the calculated isotopic ratio for each station. Equation (7) is added to the inversion as an additional constraint on the CH_4 flux estimates.

[16] The isotopic ratios used in this equation are shown in Table 1. The biomass burning source has a spatial pattern in the isotopic signature of the sources. The two primary plant photosynthetic pathways, C-3 and C-4, have differing isotopic signatures in plant biomass leading to differing isotopic signatures in emissions from combustion of C-3 and C-4 plants [*Chanton et al.*, 2000]. To account for this, a spatial map of the relative fraction of C-4 plants [*Still et al.*, 2003] and mean isotopic signatures from C-3 and C-4 plants [*Chanton et al.*, 2000] are applied to create a spatially varying isotopic signature from biomass burning. The resulting global mean isotopic signature from biomass burning is −25‰.

[17] The initial conditions were set as close to the real atmosphere as possible. First, a "test" inverse model was initialized to the observed hemispheric mean values of atmospheric CH_4 and $\delta^{13}CH_4$ [*Miller et al.*, 2002] and run from 1998 to 2000. The three-dimensional CH_4 and $\delta^{13}CH_4$ fields from the final time step of this "test" inversion are then used to initialize the inverse model. The first 3 months of the final inverse results were excluded for further model spin-up time. Three months is the time required for the modeled CH_4 mixing ratios to be further corrected by the station observations such that the differences between modeled and observed CH_4 no longer reflect inaccuracies in the initial conditions.

[18] Recent work has shown that it takes much longer to establish large-scale spatial gradients in the isotopic ratios than total CH_4 [*Tans*, 1997; *Lassey et al.*, 2000]. This implies there may be a slowly adjusting drift in the calculated atmospheric isotopic ratios due to inaccuracies in the initial conditions, which would lead to errors in the source partitioning by the inverse model. However, these errors are likely to be smaller than the errors associated with paucity of available data [*Tans*, 1997].

[19] The transport was represented by the coarse-grid version of the global, three-dimensional tracer transport model, Transport Model 3 version 3.3 (TM3) [*Heimann and Körner*, 2003], with a spatial resolution of 7.8° latitude by 10° longitude by nine vertical levels. TM3 solves the continuity equation numerically for an arbitrary number of trace gases in a three-dimensional Eulerian grid using 'off-line' wind fields. The National Centers for Weather Prediction/National Center for Atmospheric Research (NCEP/NCAR) wind fields concurrent with the model year were used. Recent model studies have suggested that a significant part of the inter-annual variability in the CH_4 growth rate may be explained by variability in model transport [*Warwick et al.*, 2002; *Johnson et al.*, 2002], implying that using meteorology corresponding to the current model year rather than repeating meteorology from a single year may be critical in correctly inferring surface fluxes from the observed CH_4 mixing ratios. Tracer transport that is resolved in the model grid is calculated using a "slopes scheme" [*Russell and Lerner*, 1981], where the distribution of each tracer within each model grid-box is represented by a three-dimensional linear slope of the mixing ratio distribution. Vertical sub-grid scale transport is calculated based on cumulus cloud convection [*Tiedke*, 1989] and vertical diffusion based on calculated air stability [*Louis*, 1979]. The ability of TM2, an earlier version of the model, and the fine grid version of TM3 to reproduce important features of tracer transport such as the interhemispheric gradient and seasonal cycle due to transport of a trace gas has been tested with SF_6, a chemically and

biologically neutral trace gas with a single, well-known anthropogenic source in the TransCom Model Intercomparison experiment [*Denning et al.*, 1999], and the role of the choice of model resolution on tracer transport in TM3 has been explored by *Heimann and Körner* [2003].

[20] The CH_4 sinks due to tropospheric OH, stratospheric loss, and oxidation by aerobic soils were prescribed and not optimized. CH_4 is oxidized by OH in the following reaction:

$$CH_4 + OH \longrightarrow CH_3 + H_2O, \quad (8)$$

which has a temperature-dependent rate constant of $k = 2.45 \times 10^{-12}\ cm^{-3}\ s^{-1} e^{-1775/T}$ [*DeMore et al.*, 1997]. The global distribution of OH was represented by the monthly OH fields of *Spivakovsky et al.* [2000], which were scaled to match the IPCC estimate of 507 Tg CH_4/yr. These OH fields have been tested for consistency with the budgets of CH_3CCl_3, a trace gas with well-known emissions that is destroyed primarily by OH oxidation, in addition to a suite of other important atmospheric trace gases [*Spivakovsky et al.*, 2000]. *Spivakovsky et al.* [2000] estimated the total uncertainty to be no greater than ±15%.

[21] The destruction of CH_4 by OH was assigned a Kinetic Isotope Effect (KIE) of 1.0054 based on the laboratory measurements of *Cantrell et al.* [1990]. A more recent measurement of this KIE of 1.0039 has been made by *Saueressig et al.* [2001]. This value is used to test the sensitivity of the inverse result to the KIE of CH_4 destruction by tropospheric OH.

[22] In addition to the tropospheric OH sink, which is responsible for approximately 88% of total CH_4 loss, CH_4 is destroyed in the stratosphere by OH, Cl, and O^1D. Owing to the large Kinetic Isotope Effect (KIE) of CH_4 destruction by Cl, the stratospheric loss term has relatively strong influence on atmospheric $\delta^{13}CH_4$ in comparison to CH_4 [*Gupta et al.*, 1996; *McCarthy et al.*, 2001]. A spatially uniform stratospheric loss term with a global total equal to the *IPCC* [2001] estimate of 40 Tg CH_4/yr was applied to all model grid cells above the temperature inversion as defined by offline temperature fields. Following *Hein et al.* [1997], total isotopic fractionation of CH_4 due to chemical destruction in the stratosphere by OH, Cl, and O^1D was assigned an isotopic discrimination of 12‰ based on observations of the correlation between $\delta^{13}CH_4$ and CH_4 in aircraft measurements [*Brenninkmeijer et al.*, 1995]. These measurements occurred near the tropopause at high southern latitudes, a region of strong transport from the stratosphere to the troposphere and are in good agreement with the observations of *Sugawara et al.* [1997]. Tropospheric Cl was not represented in the model, but recent measurements have suggested that there may be a significant active Cl sink in the boundary layer [*Platt and Hönninger*, 2003]. Owing to the large Cl KIE, this is an important source of uncertainty in the interpretation of the $\delta^{13}CH_4$ observations.

[23] The spatial distribution of the soil sink was represented by the NASA GISS field described by *Fung et al.* [1991], and the total flux was tuned to the *IPCC* [2001] emission estimate of 30 Tg CH_4/yr. An isotopic fractionation of 22‰ was assigned to the soil sink based on the measurements of *Tyler et al.* [1994]. Like the stratospheric sink, owing to its strong isotopic fractionation the soil sink has a much greater impact on the atmospheric $\delta^{13}CH_4$ than it does on total CH_4.

[24] The GLOBALVIEW-CH_4 data product based on measurements from several international laboratories was used to represent the spatiotemporal CH_4 distribution (GLOBALVIEW-CH_4 [*National Oceanic and Atmospheric Administration* (*NOAA*), 2001]). GLOBALVIEW-CH_4 is based on regular samples collected at 67 land stations and along two ocean ship tracks. The ship tracks sample 17 positions in the Pacific Ocean and seven positions in the South China Sea. The sampling sites are preferentially located to sample remote marine boundary layer air in order to ensure that the samples consist of well-mixed air, representing background mixing ratios of the trace gases measured. Duplicate samples are collected in flasks, typically once per week, and analyzed for CH_4 by gas chromatography (GC) followed by flame ionization detection (FID). The measurements are adjusted to a single scale, the NOAA Climate Monitoring Diagnostics Laboratory (NOAA CMDL) scale, in order to account for differences between individual laboratories' standard scales [*NOAA*, 2001].

[25] In order to create a temporally consistent time series over all the contributing stations, these observations are fit to a smoothed curve and the smoothed curve is sampled at regular, 7.6 day intervals. In cases where the data record is incomplete, the existing observations are extended based on the site climatology and observations from remote marine boundary sites at similar latitudes. The data extension and integration process used in GLOBALVIEW is described in more detail by *Masarie and Tans* [1995].

[26] Weekly, duplicate flask samples from six NOAA CMDL Cooperative Air Sampling Network have been sampled for $\delta^{13}CH_4$ at the Institute for Arctic and Atmospheric Research (INSTAAR) by GC isotope-ratio-mass-spectrometry (IRMS) since 1998 [*Miller et al.*, 2002]. The stations sampled for $\delta^{13}CH_4$ are Barrow, Alaska (71°N), Niwot Ridge, Colorado (40°N), Mauna Loa, Hawaii (20°N), Cape Matatula, American Samoa (14°S), Cape Grim, Tasmania (40°S), and South Pole, Antarctica (90°S). These observations are fit to a smoothed curve, excluding outliers more than 3 standard deviations from an initial smoothed curve fit. The smoothed curve is sampled at 7.6 day intervals to create a $\delta^{13}CH_4$ data set comparable to GLOBALVIEW-CH_4. It is worthy of note that trace gas observations at American Samoa are particularly difficult to interpret due to the complex tropical meteorology at this site, and this station may be especially sensitive to errors in model transport.

[27] Long-term observational records of $\delta^{13}CH_4$ are available for a number of other observing stations [e.g., *Lowe et al.*, 1994; *Quay et al.*, 1999; *Bergamaschi et al.*, 2000a]. National Institute of Water and Atmospheric Research (NIWA) observations of $\delta^{13}CH_4$ at Baring Head, New Zealand, and Scott Base, Antarctica [*Lowe et al.*, 1994], are used to validate the inverse estimates in section 6, but only the $\delta^{13}CH_4$ observations from the NOAA/CMDL network are used to constrain the inversion. The CH_4 observations from different laboratories have been carefully compared,

Table 2. Summary of the Inversion Scenarios Implemented to Compare Prior Estimates With Inverse Results and Test the Sensitivity of the Inverse Results to Various Potential Sources of Error

Scenario	Description	Additional Details
S0	a priori source estimates	forward simulation of prior source estimates shown in Table 1
S1	a posteriori estimates, excluding observations of $\delta^{13}CH_4$	inverse source estimates using CH_4 observations and prior estimates only, with no $\delta^{13}CH_4$ constraints
S2	a posteriori estimates, including observations of $\delta^{13}CH_4$	inverse source estimates with $\delta^{13}CH_4$ constraints in addition to observations of CH_4 and prior estimates
S3	sensitivity to OH kinetic isotope effect	S2 with the *Saueressig et al.* [2001] measurement of the KIE for OH
S4	sensitivity to OH fields-upper limit	S2 with OH increased by 15% to the upper end of the uncertainty estimate of *Spivakovsky et al.* [2000]
S5	sensitivity to OH field-lower limit	S2 with OH decreased 15% to the lower end of the uncertainty estimate of *Spivakovsky et al.* [2000]
S6	sensitivity to initial conditions	S2 initialized to the observed hemispheric mean CH_4 and $\delta^{13}CH_4$ for 1998 [*Miller et al.*, 2002]

adjusted to a common scale [*NOAA*, 2001], and are available as a single, self-consistent data set. Limited comparisons between NOAA/CMDL observations and data from NIWA, *Quay et al.* [1999], and *Francey et al.* [1999] suggest there may be offsets between laboratories of about 0.1‰ [*Miller et al.*, 2002], about 15% of the interhemispheric gradient. Therefore, careful measurement intercomparisons and linking of scales are essential before these data can be incorporated in the inversion to avoid introducing large biases.

[28] Inverse estimates were calculated for a variety of different "inverse scenarios," summarized in Table 2, to isolate the impact of including the $\delta^{13}CH_4$ observations and test the sensitivity of the inverse estimates to uncertainties in the model.

[29] The first scenario, S0, is simply the a priori source estimates. These source estimates have been chosen to reflect a best process-based estimate only; therefore they do not balance the CH_4 budget. S1 is the inverse estimate including only the observations of CH_4, but excluding observations of $\delta^{13}CH_4$, and S2 is the inverse model incorporating the observations of $\delta^{13}CH_4$. Throughout this paper, if the scenario being discussed is not explicitly specified, we refer to S2. Scenarios 3 to 7 test the sensitivity of the inverse model to uncertainties in OH chemistry, model transport year, and initial conditions. The base scenario, S2, uses a KIE of 5.4‰ for the oxidation of CH_4 by OH. S3 applies the more recent measurement of the OH KIE [*Saueressig et al.*, 2001]. The error associated with the OH fields used to represent the chemical sink in this study has been estimated as ±15% [*Spivakovsky et al.*, 2000]. To explore the sensitivity to this error, the OH fields have been increased uniformly by 15% in S4 and decreased by 15% in S5. Recall that the total OH sink based on the within-model CH_4 mixing ratio using the Spivakovsky OH fields of 470 Tg CH_4/yr has been adjusted to match the IPCC estimate of 507 Tg CH_4/yr, which is within the error limits of the Spivakovsky OH fields. The 15% variation for these scenarios was applied to the uncorrected value of 470 Tg CH_4/yr in keeping with the original context of the error estimate. As a result, these scenarios are expected to be asymmetric around the base scenario. Finally, in S6, the model is initialized to the observed hemispheric mean atmospheric CH_4 and $\delta^{13}CH_4$ to evaluate the sensitivity of the inverse estimates to small errors in the initial conditions after the relatively short model spin-up time [*Tans*, 1997].

3. Inverse Estimates

[30] Comparing the a priori estimates with the a posteriori estimates (Table 3) constrained by the CH_4 observations alone (S1), the largest single change is the dramatic increase

Table 3. Annual Mean Source Estimates for the A Priori Fluxes (S0) and the 1998–1999 Mean a Posteriori Estimates for the Inverse Scenarios Described in Table 2[a]

Sources	S0	S1	S2	S3	S4	S5	S6
Swamps	90	204 ± 46	206 ± 44	196 ± 44	228 ± 44	134 ± 44	200 ± 44
Bogs	50	8 ± 15	21 ± 14	22 ± 14	20 ± 14	25 ± 14	23 ± 14
Tundra	5	3 ± 4	4 ± 4	5 ± 4	4 ± 4	4 ± 4	4 ± 4
Rice agriculture	60	69 ± 18	54 ± 17	50 ± 17	56 ± 16	47 ± 17	59 ± 17
Ruminant Animals	93	94 ± 19	91 ± 18	88 ± 18	91 ± 18	89 ± 18	91 ± 18
Termites	20	36 ± 19	29 ± 18	22 ± 18	30 ± 18	24 ± 18	33 ± 18
Biomass Burning	52	65 ± 20	88 ± 18	102 ± 18	94 ± 18	68 ± 18	80 ± 18
Coal	38	30 ± 12	30 ± 11	34 ± 11	31 ± 12	28 ± 11	29 ± 11
Natural gas	57	57 ± 18	52 ± 18	56 ± 18	53 ± 18	46 ± 18	53 ± 18
Landfills	50	42 ± 14	35 ± 14	35 ± 14	36 ± 14	33 ± 14	37 ± 14
Total source	**515**	**609**	**610**	**610**	**644**	**498**	**609**

[a]Note that the relatively small ocean sources and all of the CH_4 sinks have been prescribed.

in CH_4 from swamps relative to the a priori estimates. This difference is driven by the fact that forward simulations of the a priori estimates lead to an underestimate of SH CH_4 mixing ratios compared to the observations, as shown in Figure 1. Since swamps have a strong spatial footprint in the SH and the a priori estimates for wetlands are highly uncertain, the inverse model calls for an increase in swamps to match the interhemispheric gradient. Adding the observations of $\delta^{13}CH_4$ (S2) does not significantly change this conclusion. Since the isotopic signature of wetlands is strongly depleted in ^{13}C compared to the atmosphere, this source is expected to be well constrained by the observations of atmospheric $\delta^{13}CH_4$. Therefore the observations of CH_4 and $\delta^{13}CH_4$ both strongly support an increased source from swamps. From a strictly atmospheric perspective, these features of the CH_4 observations might also be matched by a large increase in the ocean source, which was prescribed in this study, rather than an increase in swamp emissions. However, shipboard measurements of seawater and atmospheric CH_4 do not support such a dramatic increase in the oceanic CH_4 flux estimates [e.g., *Bange et al.*, 1998; *Bates et al.*, 1996; *Bange et al.*, 1994].

[31] Two recent process-model studies have also called for increased wetland spatial coverage or CH_4 flux from wetlands. Using a GCM in conjunction with a vegetation model and algorithms for determining wetland area based on topography and soil moisture, *Kaplan* [2001] estimated 11.0×10^6 km^2 of wetlands globally, about twice the spatial coverage estimated by earlier wetland inventory approaches [i.e., *Aselmann and Crutzen*, 1989; *Matthews and Fung*, 1987]. This was largely attributed to temporary wetlands that are inundated for only part of the year and are therefore not likely to be accounted for in wetland inventories. These seasonal wetlands accounted for 61% of the total wetland area estimate in this study, and over half of the seasonal wetlands occur in the tropics. Although this study does show a large increase in the spatial extent of wetlands compared to previous work, Kaplan concluded a CH_4 wetland source of 140 Tg CH_4/yr, only about 30 Tg CH_4/yr more than the inventory-based estimate of *Matthews and Fung* [1987] using a CH_4 flux estimation technique based on heterotrophic respiration. In addition to the Kaplan study, *Walter* [1998] used a process model to calculate flux from wetlands as a function of temperature and hydrological conditions, finding an unusually large source of 263 Tg CH_4/yr, even higher than that found in this top-down approach.

[32] The previous CH_4 inversions of *Hein et al.* [1997] and *Bergamaschi et al.* [2001] also found a large source from swamps. *Chen* [2004] found a lower total wetland source of 140–150 Tg CH_4/yr but very high emissions from rice cultivation of 110–120 Tg CH_4/yr. He suggested that the high inverse estimate rice paddies may be partially due to wetlands since wetlands and rice paddies have similar spatial patterns and seasonal cycles. These studies are based on different time periods than this one, so these estimates are not entirely comparable; however, they are consistent with the hypothesis that CH_4 emissions from swamps may be underestimated.

[33] The inverse flux estimates from bogs are reduced relative to the a priori sources based on the CH_4 observations alone (S1), which is not surprising since this source has a large spatial pattern in the NH, and the priors tend to overestimate sources in the NH slightly in the forward model. However, in S2, constrained by the observations of $\delta^{13}CH_4$, this source is not as greatly reduced. Like swamps, the distinctive isotopic signature of the source from bogs is expected to provide a strong constraint for this source process. A very low estimate of CH_4 from bogs from the 1998–1999 period would have been surprising since 1998 was an unusually warm year with positive precipitation anomalies over many high northern latitude land regions during the growing season [*Bell et al.*, 1999; *Curtis et al.*, 2001], and the anomalously high growth rate in 1998 has been partially attributed to increased emissions from northern wetlands resulting from these conditions [*Dlugokencky et al.*, 2001].

[34] Both S1 and S2 estimated a somewhat high source estimate for termites, although this difference is not large compared to the error estimates on the a posteriori sources. Since termites are a small, spatially diffuse source with a similar isotopic signature to wetlands, rice paddies, and ruminant animals, the station observations may not be sufficient to discriminate between this source and the other bacterial sources.

[35] As shown in Table 1, the a priori estimate for biomass burning used in this study is on the high end of the range of biomass burning estimates. This high estimate of biomass burning is consistent with the observations of CH_4, since differences between S1 and the a priori estimate are small compared to the uncertainty. The observations of $\delta^{13}CH_4$ call for an even greater biomass burning source. This source is expected to be better constrained by the observations of $\delta^{13}CH_4$ than any other source process. Like bacterial sources, biomass burning has a very distinctive isotopic signature; however, unlike these sources the isotopic signature of biomass burning is not shared by any other source process. The inverse studies of *Hein et al.* [1997], and *Bergamaschi et al.* [2001] indicated a much lower biomass burning source than this study, and the estimates of *Chen* [2004] were somewhat lower. This may be due in part to the limited use of $\delta^{13}CH_4$ observations to constrain the total CH_4 budget in these studies, the differing observational time period, or differences in inverse methodologies. *Miller et al.* [2002] and *Quay et al.* [1999] also found relatively high biomass burning sources using global mass balance calculations of CH_4 and $\delta^{13}CH_4$. In addition, recent studies have indicated that the biomass burning source may have been elevated during the period of this inversion [*Langenfelds et al.*, 2002; *Van der Werf et al.*, 2004].

[36] The landfill source estimate is reduced slightly compared to the a priori estimates by the observations of atmospheric CH_4 and reduced further by the inclusion of the $\delta^{13}CH_4$ observations. The isotopic signature of the landfill source is very close to that of the background atmosphere, so it is not constrained very well by the atmospheric isotopic data.

[37] Differences between a priori and a posteriori estimates of CH_4 emissions from tundra, rice agriculture,

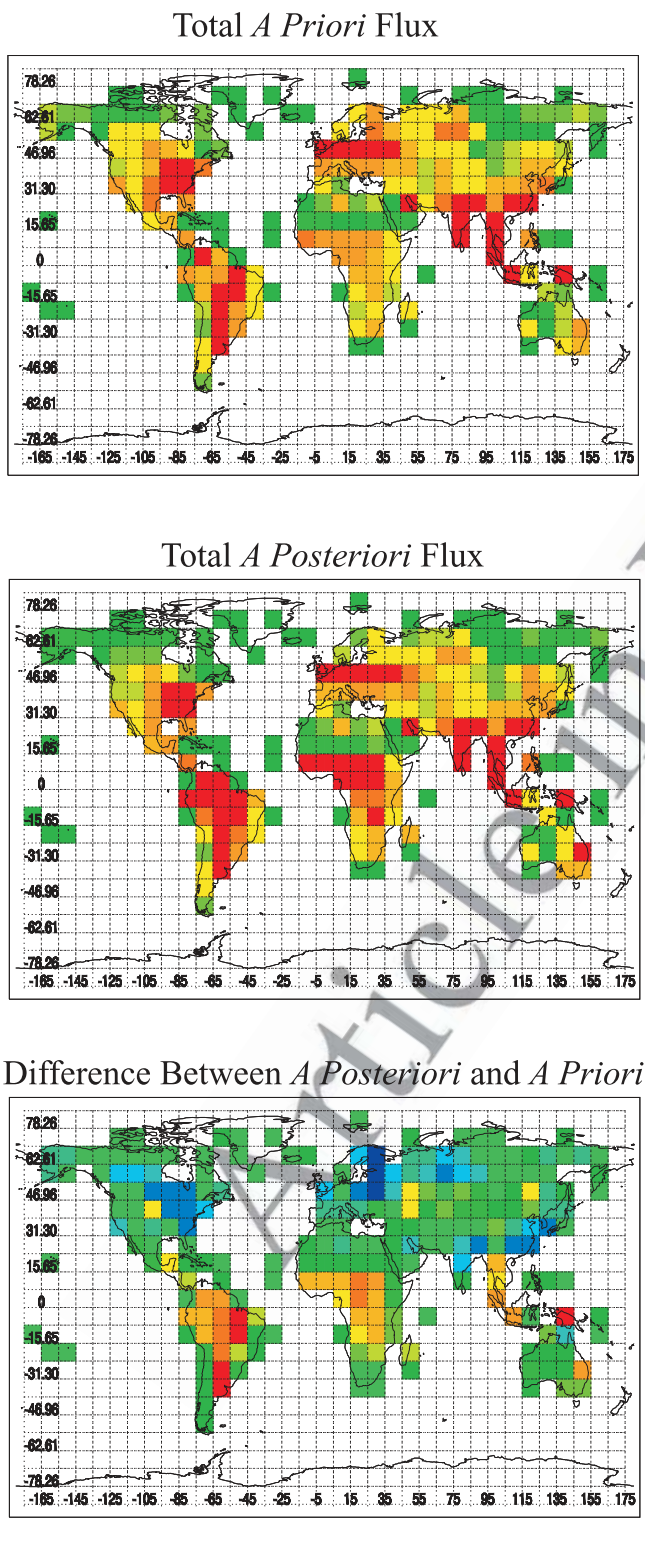

ruminant animals, coal, and natural gas are small compared to the inverse error estimates for both S1 and S2. In order to visualize the differences between the total a priori and a posteriori fluxes spatially, the emissions estimates from the source processes were used to create a total flux map by multiplying the assumed a priori spatial pattern for each source process by the corresponding inverse source estimate. Recall that we have not estimated the flux from each grid box individually. In Figure 2, the total flux maps for the a priori CH_4 flux, the a posteriori CH_4 flux (S2), and the differences between the a priori and a posteriori estimates are compared. While the small ocean source has been prescribed, there are some emissions occurring in ocean regions due to the presence of islands.

[38] Overall, the a posteriori estimates have been reduced relative to the a priori sources in the NH and increased in the SH, which is consistent with the changes expected from the interhemispheric gradient of the forward simulation in Figure 1. In North America and western Europe, the total a posteriori flux is smaller than the a priori flux, largely due to decreases in estimated emissions from landfills and coal in industrial regions and the small decrease in bogs at high northern latitudes. In eastern Eurasia, there is a slight decrease in some high-latitude regions due to the decrease in the a posteriori bog source relative to the a priori sources and an increase in midlatitudes resulting from the large increase in swamps.

[39] The spatial pattern of the difference between the a priori and a posteriori fluxes is especially interesting in Southeast Asia. In much of Asia, there is a decrease in the total a posteriori flux estimates relative to the a priori source estimates due to decreases in the emissions from rice agriculture and coal mining. However, nearby grid boxes in southern China and Indonesia show a great increase in CH_4 emissions over the a priori sources caused by the dramatic increase in the swamp source strength. This may be a bias in the model associated with the large spatial extent of the source-process regions. It is possible that the spatial pattern of swamps overestimates relative importance of the wetland contribution from these islands. However, due to the aggregation of the CH_4 fluxes to an entire source process in the inverse model, the flux from this small region must be increased proportionally to all other swamps, possibly leading to an overestimate of the flux from these islands. In order to accommodate this overestimate, the inverse model might underestimate the source from the continental rice paddies. This possibility illustrates one of the major problems associated with this type of inverse model. Since the isotopic signatures of rice paddies and swamps are similar, including the observations of $\delta^{13}CH_4$ is not likely to improve this problem.

Figure 2. Global distribution of CH_4 flux in Tg CH_4 grid cell^{-1} yr^{-1} averaged over the 1998–1999 inversion time period for (top) a priori estimates, (middle) a posteriori estimates (S2), and (bottom) the difference between the a posteriori estimates and the a priori estimates.

t4.1 **Table 4.** Hemispheric and Global Total CH_4 Fluxes of the A Priori Estimates, Inverse Estimates Constrained by the Isotopes (S2), and the Work of *Houweling et al.* [1997]

t4.2 Region	A Priori Estimates (S0)	A Posteriori Estimates (S2)	*Houweling et al.* [1999]
t4.3 NH	398	401	340
t4.4 SH	127	209	165
t4.5 NH:SH ratio	3.1	1.9	2.0
t4.6 **Global total**	**525**	**610**	**505**

748 [40] The largest increases in CH_4 flux over the a priori
749 estimates occur in South America and Africa, and are
750 primarily driven by the large increase in swamps and
751 biomass burning and secondarily affected by the larger a
752 posteriori estimates of termites and natural gas. This change
753 is in approximate agreement with the inverse CH_4 flux maps
754 of *Houweling et al.* [1999].
755 [41] The hemispheric distribution of the sources in the a
756 priori estimates, the a posteriori estimates, and the inverse
757 study of *Houweling et al.* [1999] are compared in Table 4.
758 As illustrated in more detail above, the NH:SH ratio is
759 strongly reduced by including the atmospheric observations.
760 The a posteriori NH:SH ratio used in this study is
761 remarkably similar to the values estimated by *Houweling*
762 *et al.* [1999], despite significant differences in the model
763 representation of the OH sink, inverse technique, and time
764 period of the inverse model. The Houweling study
765 [*Houweling et al.*, 1999] used a chemistry transport model
766 (CTM) tuned to match the CH_3CCl_3 observations to
767 represent the OH chemistry and a time-independent inverse
768 technique in which the inverse model was solved for each
769 model grid box rather than aggregating the model to larger
770 inverse regions. The similarities between the NH:SH ratio
771 of these very different inverse models suggests this feature
772 is robust with respect to OH loss and inverse technique and
773 strongly driven by the atmospheric data. The large
774 differences between the global total CH_4 flux estimated
775 by Houweling et al. and this study are due partly to the fact
776 that they were modeling an earlier time period (1993–1995)
777 and partly to the smaller estimate of the OH sink (450 Tg
778 CH_4/yr) by Houweling et al.

4. Interannual Variability

779
780 [42] The time period covered by these estimates coincides
781 with the anomalously large 1998 CH_4 growth rate followed
782 by a decrease in the CH_4 growth rate in 1999, so these
783 inverse results may be able to add to the discussion of the
784 causes of these anomalies. Unfortunately, the observations
785 of $\delta^{13}CH_4$ at the NOAA CMDL flask sites did not begin
786 until 1998 and the model requires 3 months of spin-up time,
787 so only 9 months of inverse results for 1998 are available.
788 Table 5 shows the mean source estimates for the last
789 9 months of 1998 and the full year of 1999. The a priori
790 sources do not vary interannually but do vary seasonally.
791 Differences between the a priori estimates listed for 1998
792 and 1999 represent the seasonal bias associated with only
793 including the last 9 months of 1998 in the average, where
794 the full year is included for 1999. The total a posteriori
795 source estimate is much larger for 1998 than 1999, due in
796 part to the seasonal bias associated with the time period
797 sampled and in part to the anomalous 1998 growth rate. In
798 the a priori sources, the April–December mean is 25 Tg
799 CH_4/year higher than the annual average. In addition, the
800 1998 growth rate increase corresponds to an increase of
801 ~24 Tg CH_4/yr in the imbalance between CH_4 sources and
802 sinks compared to the earlier 1995–1997 time period
803 [*Dlugokencky et al.*, 2001]. Between 1998 and 1999, the
804 global observed growth rate decreased from 12.7 ppb to
805 2.6 ppb, indicating a corresponding decrease in the source/
806 sink imbalance.
807 [43] Currently, there are two competing hypotheses
808 regarding the 1998 growth rate anomaly. On the basis of
809 careful analysis of the methane growth rate and a process
810 model experiment, *Dlugokencky et al.* [2001] suggested that
811 the 1998 growth rate increase was due to increased flux
812 from wetlands as a result of the temperature and precipita-
813 tion anomalies. Conversely, a recent multispecies analysis
814 study suggested that a great deal of the 1998 CH_4 growth

t5.1 **Table 5.** Mean A Priori and A Posteriori Flux Estimates of CH_4 Flux for April–December 1998 and All of 1999[a]

t5.2 Sources	A Priori Estimates April–Dec. Mean, Tg CH_4/yr	A Posteriori (S2) 1998 April–Dec. Mean, Tg CH_4/yr	A Priori Estimates Annual Mean, Tg CH_4/yr	A Posteriori (S2) 1999 Annual Mean, Tg CH_4/yr
t5.3 Swamps	92	221 ± 44	90	208 ± 44
t5.4 Bogs	61	30 ± 13	50	12 ± 143
t5.5 Tundra	7	12 ± 4	5	0 ± 4
t5.6 Rice agriculture	71	53 ± 17	60	56 ± 17
t5.7 Ruminant animals	93	97 ± 18	93	87 ± 18
t5.8 Termites	20	48 ± 18	20	16 ± 18
t5.9 Biomass Burning	51	91 ± 18	52	88 ± 20
t5.10 Coal	38	15 ± 11	38	40 ± 11
t5.11 Natural gas	57	49 ± 18	57	62 ± 18
t5.12 Landfills	50	34 ± 14	50	31 ± 14
t5.13 **Total source**	**540**	**646**	**515**	**601**

[a]Note that the a priori source estimates do not include interannual variability. The differing a priori sources from 1998 to 1999
t5.14 reflect the seasonality of the sources since the two time-averaged values include different months.

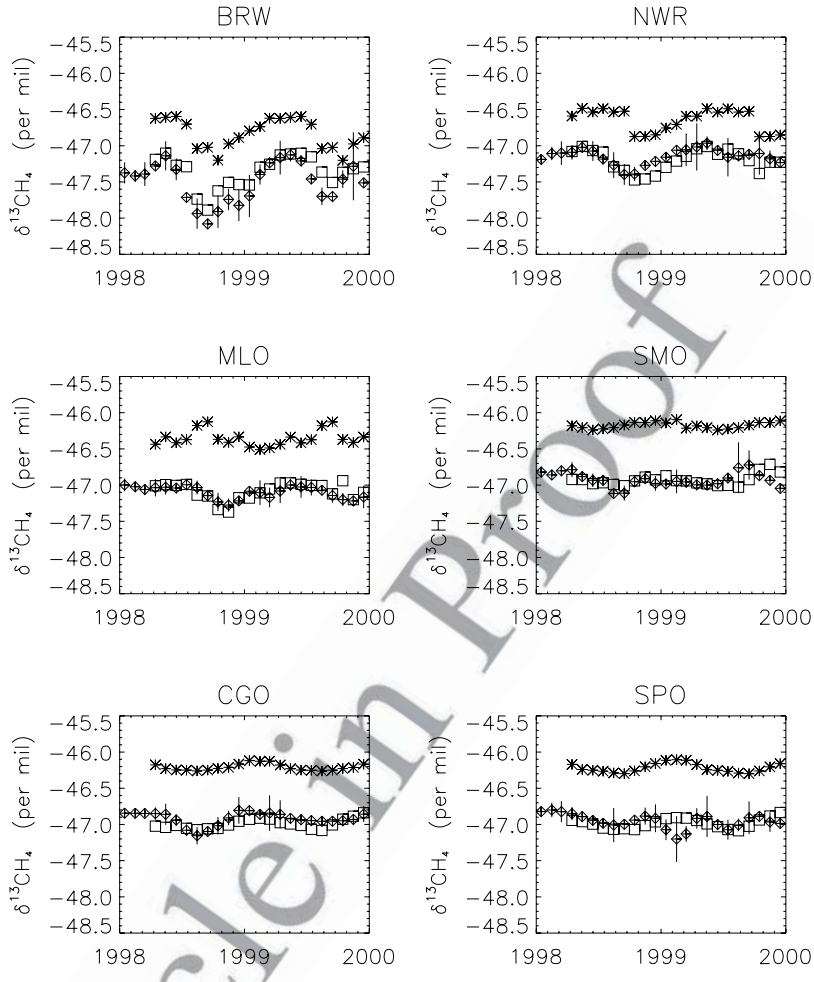

Figure 3. Comparison between the monthly mean $\delta^{13}CH_4$ measurement record at six observing stations (diamonds), model simulation based on a priori sources (asterisks), and the model simulation based n the a posteriori sources (squares). The observing stations shown are Barrow, Alaska (BRW), Niwot Ridge, Colorado (NWR), Mauna Loa, Hawaii (MLO), Tutuila, American Samoa (SMO), Cape Grim, Tasmania (CGO), and South Pole, Antarctica (SPO). Error bars on the measurements represent the standard deviation of the individual observations from the smoothed curve.

rate anomaly was caused by biomass burning rather than wetlands based on correlations between atmospheric observations of CO_2 and it's $\delta^{13}C$, H_2, CH_4, and CO [*Langenfelds et al.*, 2002]. In addition, *Van der Werf et al.* [2004] also attributed much of the CH_4 anomaly to biomass burning based on satellite observations of fires combined with atmospheric models, CO observations, and observed emission rations.

[44] The results of this inversion support the conclusions of *Dlugokencky et al.* [2001] that a large portion of the 1998 growth rate anomaly was due to an unusually large wetland source. The large change between 1998 and 1999 occur in the wetland sources including swamps, bogs, and tundra, although the interannual variations in swamps and bogs are not far larger than the error estimates and should be interpreted with caution. In addition, the large change in the termite source, which is not consistent with process-level understanding of the interannual variability of termite emissions, is most likely due to variability in the wetland source. Since the termite source has a similar isotopic signature to wetlands and a somewhat similar spatial footprint to swamps, it is possible that the inverse model is not effectively partitioning these two sources and part of this variability is actually due to wetlands. The magnitude of the 1998–1999 wetland variations is also in reasonable agreement with the process model simulations of Dlugokencky et al. regarding the anomaly. Using a global process-based model that includes soil temperature and moisture, they calculated an emission anomaly of 11.6 Tg CH_4/yr for wetlands north of 30°N and 13 Tg for tropical wetlands.

[45] There is very little variation in the biomass burning estimate between these two model years. However, it is likely that fires played an important role in the increasing growth rate at the end of 1997 and perhaps the beginning of 1998, consistent with the Langenfelds study [*Langenfelds et al.*, 2002]. There was an anomalous wildfire source from peat fires in Asia at the end of 1997, resulting in a large perturbation to the carbon cycle [*Page et al.*, 2002], but this event is not observed in these results, since 1997 and the

early months of 1998 were not included in these estimates. In addition, owing to the large uncertainty estimates associated with this work, these results do not preclude a moderate biomass burning anomaly in addition to large wetland fluxes during 1998. For example, if OH was lower in 1998 than 1999 [e.g., *Novelli et al.*, 2003], the ratio of bacterial sources to biomass burning sources might also be overestimated in 1998 and/or underestimated in 1999, since OH enriches atmospheric CH_4 in ^{13}C.

[46] The reason that the inversion attributed the bulk of the 1998–1999 variability to bacterial sources rather than biomass burning can be found in the observational record of $\delta^{13}CH_4$ (Figure 3). If this anomaly were primarily due to biomass burning, one would expect to see a peak in the observations of $\delta^{13}CH_4$ to reflect the relatively heavy isotopic signature of this source. Instead, more negative $\delta^{13}CH_4$ isotopic signatures were observed at Barrow, Alaska, Mauna Loa, Hawaii, and Cape Grim, Tasmania, in late 1998. Therefore the observations used to constrain this model call for greater fluxes from sources with lighter isotopic signatures than the background atmosphere in 1998, resulting in high estimates of bacterial sources.

[47] Two hypothetical model scenarios were used to examine how well the observations of CH_4 and $\delta^{13}CH_4$ might be able to constrain a biomass burning anomaly. The 1998 anomaly reflects to a source/sink imbalance of 24 Tg CH4 [*Dlugokencky et al.*, 2001]. In one biomass burning scenario, the entire anomaly is attributed to biomass burning by increasing the a posteriori biomass burning by 24 Tg CH_4 in 1998 and reducing the a posteriori wetland source by an equal amount. The second scenario reflects the effect of attributing one third of the total anomaly to biomass burning and the remainder to wetlands, following the results of an earlier analysis of $\delta^{13}CH_4$ [*Miller et al.*, 2002].

[48] These scenarios were constructed by combining *the a posteriori* CH_4 and $\delta^{13}CH_4$ mixing ratios with CH_4 and $^{13}CH_4$ mixing ratios calculated by forward model simulations of a 1998 biomass burning perturbation, $[CH_4]_{BB\ pert}$, and a 1998 wetland perturbation, $[CH_4]_{BB\ pert}$, in which both perturbations include OH loss. The resulting concentrations of CH_4 and $^{13}CH_4$ can be written as

$$[CH_4]_{Scenario} = [CH_4]_{a\ posteriori} + [CH_4]_{BB\ pert} - [CH_4]_{Wetl.\ pert} \quad (9)$$

$$\left[^{13}CH_4\right]_{Scenario} = \left[^{13}CH_4\right]_{a\ posteriori} + \left[^{13}CH_4\right]_{BB\ pert} - \left[^{13}CH_4\right]_{Wetl.\ pert}. \quad (10)$$

Then the $\delta^{13}CH_4$ for the new scenario is calculated following equation (4).

[49] A 24 Tg CH4 increase in the biomass burning source and a corresponding decrease in the wetland source during 1998 would result in a significant change in the $^{13}C/^{12}C$ isotopic ratio of atmospheric CH_4 at most observing stations, but very little change in the CH_4 mixing ratio, as shown for MLO in Figure 4. At the end of 1998, the atmospheric $\delta^{13}CH_4$ for this scenario is between 0.16 and 0.23 per mil higher than the a posteriori isotopic signature

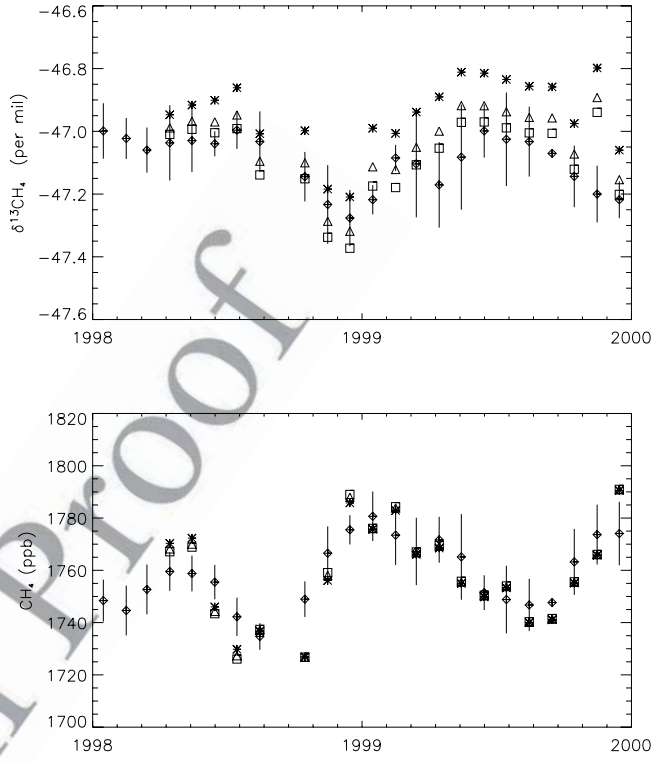

Figure 4. Comparison between the monthly mean (top) $\delta^{13}CH_4$ and (bottom) CH_4 measurement record at MLO (diamonds), model simulation based on a posteriori sources (squares), and two scenarios which explore the effect of a 1998 biomass burning anomaly on atmospheric $\delta^{13}CH_4$ and CH_4. In once scenario, the entire 1998 anomaly was attributed to biomass burning by reducing the a posteriori wetland source by 24 Tg CH_4 during 1998 and increasing the a posteriori biomass burning source by the same amount (asterisks). Then, the possibility of an anomaly due to a combination of increased biomass burning and wetland emissions was examined by reducing the a posteriori wetland source by 8 Tg CH_4 during 1998 and increasing the a posteriori biomass burning source by the same amount (triangles). Error bars on the measurements represent the standard deviation of the individual observations from the smoothed curve.

for the three NH stations and between 0.02 and 0.16 per mil higher for the SH stations. At MLO, NWR, and SMO, the difference between the a posteriori $\delta^{13}CH_4$ and the new scenario during 1999 is close to the magnitude of the seasonal cycle. Conversely, the second scenario, in which only one third of the total anomaly is shifted to biomass burning, is still reasonably consistent with the observations (Figure 4). This simulation combined with the error estimate associated with the a posteriori biomass burning flux indicates that the observations used to constrain the inverse model are consistent with moderate contribution of biomass burning to the 1998 growth rate anomaly.

[50] The simulated CH_4 concentrations are very similar for the a posteriori case and both biomass burning scenarios (Figure 4, bottom), as would be expected based

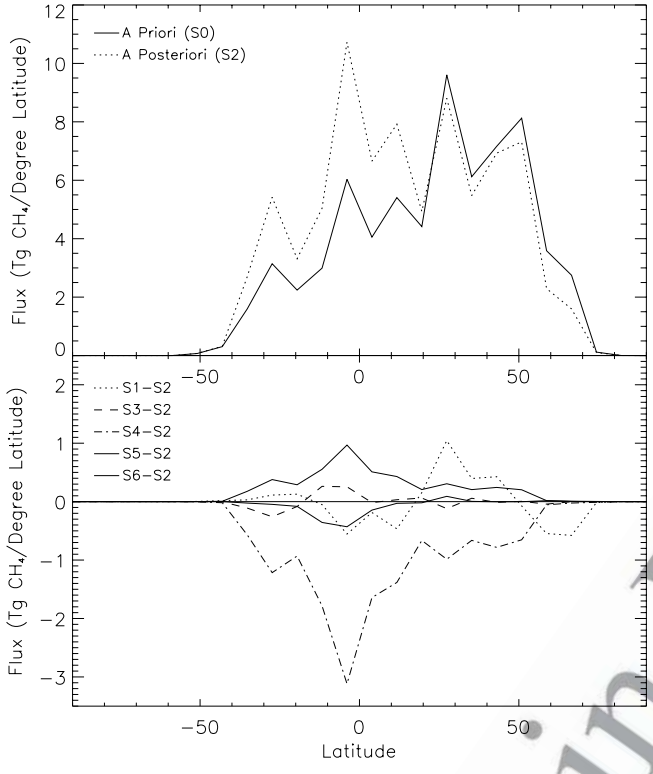

Figure 5. (top) Latitudinal gradient of the a priori and a posteriori CH_4 flux estimates and (bottom) the difference between the a posteriori flux estimates for the inverse scenarios described in Table 2 and the standard inverse scenario, S2.

on the work of *Fung et al.* [1991]. This suggests that a 24 Tg CH_4 perturbation from biomass burning perturbation would be very difficult to distinguish from a similar perturbation due to wetlands based on the observations of CH_4 alone. Observations of $\delta^{13}CH_4$ provide far more insight into the source processes controlling changes of this magnitude.

[51] The changes in landfills, natural gas, coal, ruminant animals, and termites between 1998 and 1999 probably primarily reflect model noise as a function of time. These sources do not have significant seasonal variations, so seasonal bias issues do not apply to these sources. In addition, large variability on annual timescales is unlikely for these sources. For example, while the ruminant animal source is likely to change significantly with changes in feed quality, age demographics of the animals, and other factors, these kinds of changes on a global scale are not likely to occur over a 2-year time period.

5. Sensitivity of the Results

[52] In order to determine whether the major conclusions of this study are robust with respect to several sources of uncertainty, inverse estimates have been calculated after varying a number of model features in scenarios 3–7, summarized in Table 2. The results of these sensitivity tests are compared to the base scenario, S2, in Table 3 and Figure 5 (bottom).

[53] Overall, the major conclusions of the inverse study are reasonably robust with respect to changes in these model parameters. Changing the KIE of CH_4 oxidation by OH (S3) had very little effect on the inverse results. The differences between S2 and S3 never exceed the error bars of the inverse estimates. The largest percent difference between these two model runs is the biomass burning source, which changes by 14%. Since the smaller OH KIE results in less enrichment in atmospheric ^{13}C from the chemical sink, the inverse model calls for more biomass burning, since the biomass burning source is very enriched compared to the atmosphere. Since bacterial sources deplete the atmosphere in ^{13}C, most of the bacterial sources are reduced slightly between S2 and S3. Because OH concentrations are much higher low latitudes, the largest perturbations to the emissions under this scenario occur in the tropics (Figure 5), and emissions from bogs and tundra, which occur predominantly at high latitudes, increased slightly in S3 rather than decreasing.

[54] S4 and S5 test the upper and lower limits of the OH fields, as determined by *Spivakovsky et al.* [2000]. Recall that the lower limit test (S4) is expected to diverge more from S2 than the upper limit test (S5) because the base scenario is closer to the high end of the range. In both the upper and lower limit, the global total CH_4 source strength changes significantly, since the total magnitude of the sink is changed relative to the base scenario while the amount of CH_4 in the atmosphere remains unchanged, with the greatest changes occurring for sources with large emissions in the tropics (Figure 6). The upper limit OH estimate results in very little divergence from the base scenario for most sources, but does result in increased emissions from biomass burning and swamps. Applying the lower limit OH sink to the inversion (S5) results in large changes in the inverse flux estimates in the tropics (Figure 5). The largest decrease occurs in swamps; however, even with this decrease, the inverse model still calls for a large increase in this source compared to the a priori source estimates. A corresponding large change occurs in biomass burning, showing that the relatively high estimates of biomass burning found in this study are not robust in the lower limit of OH production. Changes to the other source strength estimates are small relative to the error estimates. The strong perturbations to the CH_4 emissions from swamps and biomass burning relative to the other source processes are probably due to the fact that destruction by OH is the greatest in the tropics, and these two source processes occur largely in the tropics, while their isotopic signatures have opposite effects on the atmosphere. Therefore, decreasing both sources corrects for the OH perturbation while matching the $\delta^{13}CH_4$ observations. Finally, the changes in the source estimates from a large change in initial conditions are small.

[55] Overall, the most of the conclusions from the previous section are robust with respect to these changes in the model parameters tested here, but the a posteriori flux estimates are sensitive to large changes in OH. Since the OH sink is the largest single component of the CH_4

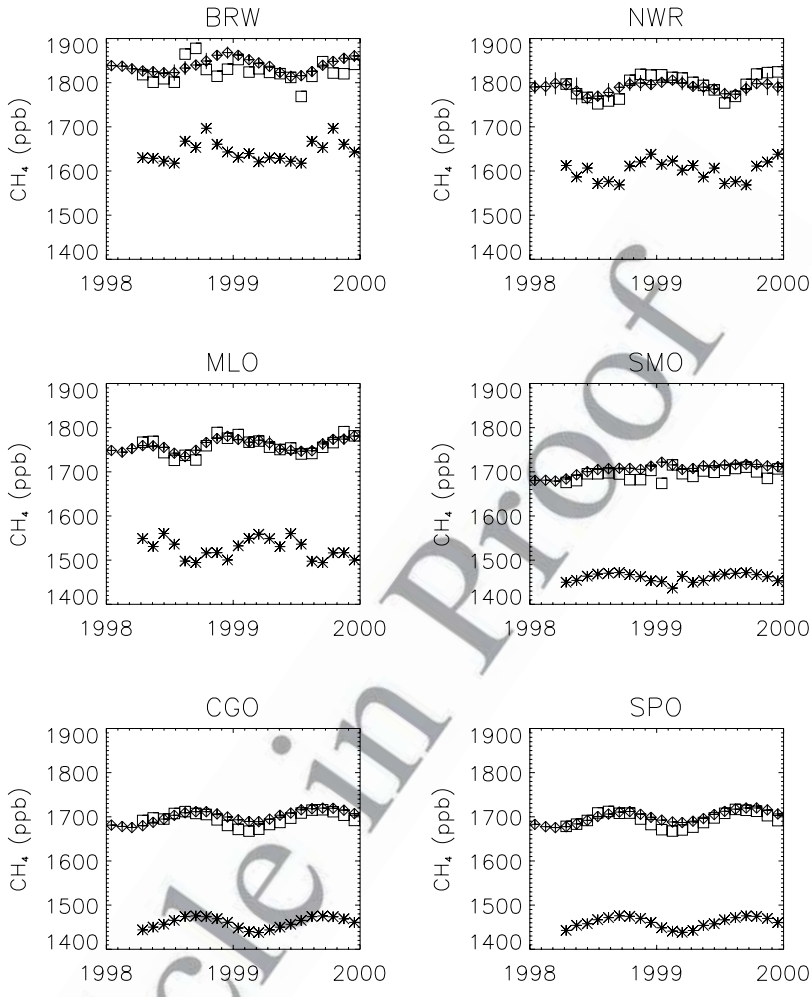

Figure 6. Comparison between the monthly mean CH_4 measurement record at six observing stations (diamonds), model simulation based on a priori sources (asterisks), and the model simulation based on the a posteriori sources (squares). Error bars on the measurements represent the standard deviation of the individual observations from the smoothed curve.

budget, and changing the fractionation of this sink by 1.5‰ did not significantly change the inverse estimates, the results shown here are not expected to be strongly sensitive to small changes in the isotopic signatures of the sources.

6. A Posteriori Atmospheric CH_4 Mixing Ratios and $\delta^{13}CH_4$

[56] One advantage of inverse source estimates is that they are constrained by the observations of the trace gas in the atmosphere. Therefore forward simulations using the inverse estimates should reproduce the broad features of the observations such as the interhemispheric gradient and seasonal cycle at observing stations well. Figures 1, 3, and 6 compare the modeled CH_4 and $\delta^{13}CH_4$ based on the a posteriori sources to those based on a priori sources to the observational record at the stations used to constrain the inversion. Figure 7 compares the a posteriori $\delta^{13}CH_4$ with the observational record from two NIWA stations that were not used to constrain the inversion, Baring Head, New Zealand, and Scott Base, Antarctica [*Lowe et al.*, 1994], as an independent validation of the inverse model.

[57] The inverse sources match the observed latitudinal gradients of both CH_4 and $\delta^{13}CH_4$ well, especially in comparison to the a priori estimates (Figure 1). There are two stations that have very high observed values compared to other stations at similar latitudes, which are not well matched by the inverse estimates. These stations, located on the Black Sea in Romania (BSC) and Cape Rama, India (CRI), are likely to be influenced by the large continental sources nearby. The observations at stations sampling continental air were given a higher uncertainty than observations at stations sampling marine air, implying that stations sampling continental air do not constrain the inverse model as strongly as those sampling marine air. The reason for weighting these stations more weakly in the inversion is that these data are influenced more strongly by

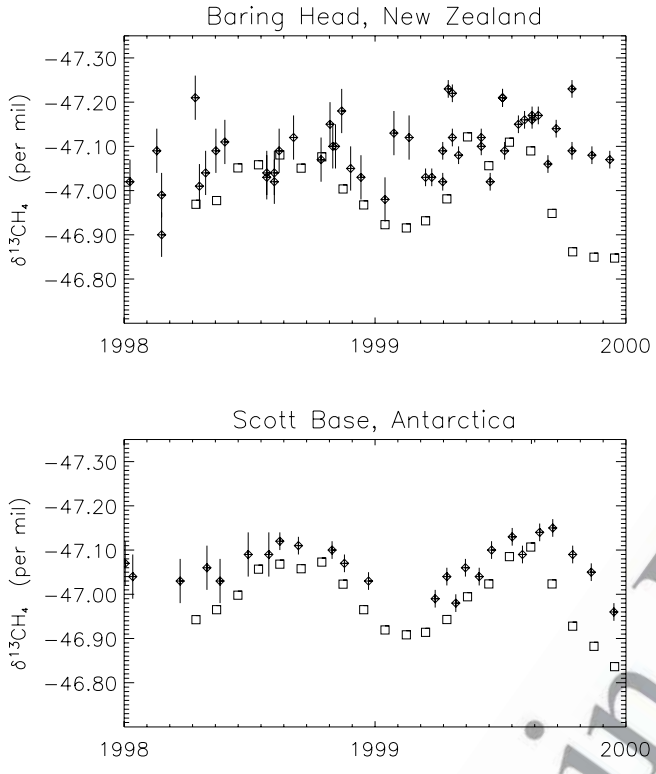

Figure 7. Comparison between the $\delta^{13}CH_4$ measurement (diamonds) and the model simulation based on the a posteriori sources (squares) for two NIWA observing stations: Baring Head, New Zealand, and Scott Base, Antarctica [*Lowe et al.*, 1994].

local sources, small-scale transport effects, and other factors that cannot be represented effectively in a coarse resolution model. The a posteriori CH_4 does not reproduce observations at BSC and CRI well because they are weighted more weakly, and a linear combination of large source regions that matched these stations well would not be consistent with the other station observations.

[58] The monthly mean observations and model results are compared at the six NOAA CMDL stations where both observations of CH_4 and observations of $\delta^{13}CH_4$ are made (Figures 3 and 5). Overall, the a posteriori estimates match the broad features of the CH_4 and $\delta^{13}CH_4$ observations at these stations, as well as at the two NIWA stations that were not used to constrain the inverse model (Figure 7).

[59] In all cases, the a posteriori CH_4 source estimates result in a far better match to the station observations than the a priori estimates. The a posteriori correct the a priori underestimate of the overall magnitude of the CH_4 mixing ratio as well as the poor match to the a priori seasonal cycle at BRW and MLO. There is a small a posteriori overestimate of CH_4 at NWR at the end of 1998. The use of large spatial regions and coarse model resolution can sometimes preclude an exact match to the station observations based on linear combinations of these large regions, and this may have caused this discrepancy. The a posteriori calculation of atmospheric $\delta^{13}CH_4$ generally matches the mean observed $\delta^{13}CH_4$ and the observed $\delta^{13}CH_4$ seasonal cycle, as accurately as the CH_4 match.

7. Conclusions

[60] We have presented source estimates that are optimally consistent with the observations of atmospheric CH_4 and $\delta^{13}CH_4$ and process-level understanding of the sources and sinks. There are many important departures from previous source estimates. The CH_4 source from wetlands was unusually large, which agrees with two recent process-level models suggesting a greater importance of wetland ecosystems than previously thought [*Kaplan*, 2001; *Walter*, 1998]. The interannual distribution of this source supports the hypothesis of *Dlugokencky et al.* [2001] that the 1998 growth rate anomaly was primarily caused by increased wetland emissions. Biomass burning source estimates were very high, in agreement with an earlier study incorporating observations of $\delta^{13}CH_4$ [*Miller et al.*, 2002].

[61] These results show that through inverse modeling, the atmospheric CH_4 and $\delta^{13}CH_4$ observations have the capacity to add unique insight into the CH_4 problem, but significant limitations to this technique persist. While the inverse results are robust with respect to changes in the initial conditions and the OH KIE, the CH_4 flux estimates for biomass burning and swamps are sensitive to changes in the assumed OH sink. The inverse estimates may also be sensitive to inaccuracies in model transport and the assumed isotopic signature of the sources. The aggregation of the sources into spatially diffuse source process regions introduces both a source of error and a limitation to the understanding that may be provided by the inverse estimates. The error is introduced by the assumption that the CH_4 flux can be represented by a linear combination of a small number of source regions and that the assumed spatial pattern of the CH_4 emissions within these regions are perfect. In reality, the spatial distributions of many of the source processes are likely to vary with regional temperature anomalies and other physical processes. In addition, grouping the sources in this way removes the potential to use the CH_4 and $\delta^{13}CH_4$ observations to diagnose changes in CH_4 flux on regional scales.

Appendix A: Derivation of Equation (5)

[62] First, equation (3) is divided by an arbitrary reference ratio of $^{13}C/^{12}C$.

$$\frac{R_j^{\text{obs}}}{R_{\text{reference}}} y_j^{\text{obs}} - \frac{R_j}{R_{\text{reference}}} y_j = \sum_{i=1,\text{nsrc}} \mathbf{H}_{i,j} \frac{R_i}{R_{\text{reference}}} x_i. \qquad \text{(A1)}$$

Then, equation (2) is subtracted from equation (A1).

$$\left(\frac{R_j^{\text{obs}}}{R_{\text{reference}}} y_j^{\text{obs}} - y_j^{\text{obs}}\right) - \left(\frac{R_j}{R_{\text{reference}}} y_j - y_j\right) = \sum_{i=1,nsrc} \mathbf{H}_{i,j} \frac{R_i}{R_{\text{reference}}} x_i - \sum_{i=1,\text{nsrc}} \mathbf{H}_{i,j} x_i. \qquad \text{(A2)}$$

Equation (A2) is multiplied by 1000 and rearranged.

$$\left(\frac{R_j^{\text{obs}}}{R_{\text{reference}}} - 1\right) \times 1000 \times y_j^{\text{obs}} - \left(\frac{R_j}{R_{\text{reference}}} - 1\right) \times 1000 \times y_j = \sum_{i=1,\text{nsrc}} \mathbf{H}_{i,j} x_i \times \left(\frac{R_i}{R_{\text{reference}}} - 1\right) \times 1000. \quad \text{(A3)}$$

Finally, equation (4), the definition of δ units, can be substituted into equation (A3) to reach equation (5).

$$\delta_j^{\text{obs}} y_j^{\text{obs}} - \delta_j y_j = \sum_{i=1,\text{nsrc}} \mathbf{H}_{i,j} x_i \delta_i.$$

[63] **Acknowledgments.** We thank Jim White, Scott Denning and A. R. Ravishankara for their insightful comments and helpful discussions. We are especially grateful to all of the scientists responsible for the observations that made this work possible, including all of the contributors to the Cooperative Air Sampling Network and the Carbon Cycle Greenhouse Gases Group at NOAA. In particular, we thank Jim White and INSTAAR for the measurements of $\delta^{13}CH_4$ and Ken Masarie for his work on the GLOBALVIEW data product. The authors also acknowledge Dave Lowe, Gordon Brailsford, and Ross Martin for the $\delta^{13}CH_4$ observations at Baring Head, New Zealand, and Scott Base, Antarctica. S. F., P. T., L. B., and J. M. acknowledge the NOAA Office of Oceanic and Atmospheric Research for support. S. F. also acknowledges CIRES for support through the Graduate Research Fellowship program and the Biosphere Atmosphere Stable Isotope Network (BASIN) for travel funding that facilitated the development of this work. This research has also been presented in S. F.'s doctoral dissertation at the University of Colorado, Boulder, Colorado, USA, 2003.

References

Aselmann, I., and P. J. Crutzen (1989), Global distribution of natural freshwater wetlands and rice paddies, their net primary productivity, seasonality, and possible methane emissions, *J. Atmos. Chem.*, *8*, 307–358.

Bange, H. W., U. H. Bartell, S. Rapsomanikis, and M. O. Andreae (1994), Methane in the Baltic and North Seas and a reassessment of the marine emissions of methane, *Global Biogeochem. Cycles*, *8*, 465–480.

Bange, H. W., R. Ramesh, S. Rapsomanikis, and M. O. Andreae (1998), Methane in surface waters of the Arabian Sea, *Geophys. Res. Lett.*, *25*, 3547–3550.

Bates, T. S., K. C. Kelly, J. E. Johnson, and R. H. Gammon (1996), A reevaluation of the open ocean source of methane to the atmosphere, *J. Geophys. Res.*, *101*, 6953–6961.

Bekki, S., K. S. Law, and J. A. Pyle (1994), Effect of ozone depletion on atmospheric CH_4 and CO concentrations, *Nature*, *371*, 595–597.

Bell, G. D., M. S. Halpert, C. F. Ropelewski, V. E. Kousky, A. V. Douglas, R. C. Schnell, and M. E. Gelman (1999), Climate assessment for 1998, *Bull. Am. Meteorol. Soc.*, *80*, S1–S48.

Bergamaschi, P., M. Bräunlich, T. Marik, and C. A. M. Brenninkmeijer (2000a), Measurements of the carbon and hydrogen isotopes of atmospheric methane at Izaña, Tenerife: Seasonal cycles and synoptic-scale variations, *J. Geophys. Res.*, *105*, 14,531–14,546.

Bergamaschi, P., R. Hein, M. Heimann, and P. J. Crutzen (2000b), Inverse modeling of the global CO cycle: 1. Inversion of CO mixing ratios, *J. Geophys. Res.*, *105*, 1909–1927.

Bergamaschi, P., D. C. Lowe, M. R. Manning, R. Moss, T. Bromley, and T. S. Clarkson (2001), Transects of atmospheric CO, CH_4, and their isotopic composition across the Pacific: Shipboard measurements and validation of inverse models, *J. Geophys. Res.*, *106*, 7993–8011.

Bingemer, H. G., and P. J. Crutzen (1987), The production of methane from solid wastes, *J. Geophys. Res.*, *92*, 2181–2187.

Brenninkmeijer, C. A. M., D. C. Lowe, M. R. Manning, R. J. Sparks, and P. F. J. van Velthoven (1995), The ^{13}C, ^{14}C, and ^{18}O isotopic composition of CO, CH_4, and CO_2 in the higher southern latitudes lower stratosphere, *J. Geophys. Res.*, *100*, 26,163–26,172.

Bruhwiler, L., P. Tans, and M. Ramonet (2000), A time-dependent assimilation and source retrieval technique for atmospheric tracers, in *Inverse Methods in Global Biogeochemical Cycles*, *Geophys. Monogr. Ser.*, vol. 114, edited by P. Kasibhatla et al., pp. 265–277, AGU, Washington, D. C.

Cantrell, C. A., R. E. Shetter, A. H. McDaniel, J. G. Calvert, J. A. Davidson, D. C. Lowe, S. C. Tyler, R. J. Cicerone, and J. P. Greenberg (1990), Carbon kinetic isotope effect in the oxidation of methane by the hydroxyl radical, *J. Geophys. Res.*, *95*, 22,455–22,462.

Chanton, J. P., C. M. Rutkowski, C. C. Schwartz, D. E. Ward, and L. Boring (2000), Factors influencing the stable isotope signature of methane from combustion and biomass burning, *J. Geophys. Res.*, *105*, 1867–1877.

Chen, Y.-H. (2004), Estimation of methane and carbon dioxide surface fluxes using a 3-D global atmospheric chemical transport model, Ph.D. thesis, Mass. Inst. of Technol., Cambridge, Mass.

Cicerone, R. J., and R. S. Oremland (1988), Biogeochemical aspects of atmospheric methane, *Global Biogeochem. Cycles*, *2*, 299–327.

Curtis, S., R. Adler, G. Huffman, E. Nelkin, and D. Bolvin (2001), Evolution of tropical and extratropical precipitation anomalies during the 1997–1999 ENSO Cycle, *Int. J. Climatol.*, *21*, 961–967.

DeMore, W. B., S. P. Sander, D. M. Golden, R. F. Hampson, M. J. Kurylo, C. J. Howard, A. R. Ravishankara, C. E. Kolb, and M. J. Molina (1997), Chemical kinetics and photochemical data for use in stratospheric modeling, *Publ. 97-4*, Jet Propulsion Lab., Pasadena, Calif.

Denning, S. A., et al. (1999), Three-dimensional transport and concentration of SF6: A model intercomparison study (Transcom 2), *Tellus*, *Ser. B*, *51*, 266–297.

Dlugokencky, E. J., E. G. Dutton, P. C. Novelli, P. P. Tans, K. A. Masarie, K. O. Lantz, and S. Madronich (1996), Changes in CH_4 and CO growth rates after the eruption of Mt. Pinatubo and their link with changes in tropical tropospheric UV flux, *Geophys. Res. Lett.*, *23*, 2761–2764.

Dlugokencky, E. J., K. A. Masarie, P. M. Lang, and P. P. Tans (1998), Continuing decline in the growth rate of the atmospheric methane burden, *Nature*, *393*, 447–450.

Dlugokencky, E. J., B. P. Walter, K. A. Masarie, P. M. Lang, and E. S. Kasischke (2001), Measurements of an anomalous global methane increase during 1998, *Geophys. Res. Lett.*, *28*, 499–502.

Dlugokencky, E. J., S. Houweling, L. Bruhwiler, K. A. Masarie, P. M. Lang, J. B. Miller, and P. P. Tans (2003), Atmospheric methane levels off: Temporary pause or a new steady state?, *Geophys. Res. Lett.*, *30*(19), 1992, doi:1029/2003GL017475.

Enting, I. G., and J. V. Mansbridge (1989), Seasonal sources and sinks of atmospheric CO_2: Direct inversion of filtered data, *Tellus*, *Ser. B*, *41*, 111–126.

Etheridge, D. M., L. P. Steele, R. J. Francey, and R. L. Langenfelds (1998), Atmospheric methane between 1000 A.D. and present: Evidence of anthropogenic emissions and climatic variability, *J. Geophys. Res.*, *103*, 15,979–15,993.

Fan, S. M., M. Gloor, J. Mahlman, S. Pacala, J. Sarmiento, T. Takahashi, and P. Tans (1998), A large terrestrial carbon sink in North America implied by atmospheric and oceanic carbon dioxide data and models, *Science*, *282*, 442–446.

Fiore, A. M., D. J. Jacob, B. D. Field, D. G. Streets, S. D. Fernandes, and C. Jang (2002), Linking ozone pollution and climate change: The case for controlling methane, *Geophys. Res. Lett.*, *29*, 1919–1923.

Francey, R. J., M. R. Manning, C. E. Allison, S. A. Coram, D. M. Etheridge, R. L. Langenfelds, D. C. Lowe, and L. P. Steele (1999), A history of $\delta^{13}C$ in atmospheric CH_4 from the Cape Grim Air Archive and Antarctic firn air, *J. Geophys. Res.*, *104*, 23,631–23,643.

Fung, I., J. John, J. Lerner, E. Matthews, M. Prather, L. P. Steele, and P. J. Fraser (1991), Three-dimensional model synthesis of the global methane cycle, *J. Geophys. Res.*, *96*, 13,033–13,065.

Gupta, M., S. Tyler, and R. Cicerone (1996), Modeling atmospheric $\delta^{13}CH_4$ and the causes of recent changes in atmospheric CH_4 amounts, *J. Geophys. Res.*, *101*, 22,923–22,932.

Gurney, K. R., et al. (2002), Towards robust regional estimates of CO_2 sources and sinks using atmospheric transport models, *Nature*, *415*, 626–630.

Heimann, M., and S. Körner (2003), The Global Atmospheric Tracer Model TM3 model description and user's manual, technical report, Max-Planck-Inst. für Biogeochem., Jena, Germany.

Hein, R., P. J. Crutzen, and M. Heimann (1997), An inverse modeling approach to investigate the global atmospheric methane cycle, *Global Biogeochem. Cycles*, *11*, 43–76.

Houweling, S., T. Kaminski, F. Dentener, J. Lelieveld, and M. Heimann (1999), Inverse modeling of methane sources and sinks using the adjoint of a global transport model, *J. Geophys. Res.*, *104*, 26,137–26,160.

Intergovernmental Panel on Climate Change (2001), *Climate Change 2001: The Scientific Basis*, edited by J. T. Houghton et al., Cambridge Univ. Press, New York.

Johnson, C. E., D. S. Stevenson, W. J. Collins, and R. G. Derwent (2002), Interannual variability in methane growth rate simulated with a coupled

ocean-atmosphere-chemistry model, *Geophys. Res. Lett.*, *29*, 1903–1907.
Jones, R. L., and J. A. Pyle (1984), Observations of CH_4 and N_2O by the Nimbus 7 SAMS: A comparison with in situ data and two-dimensional numerical model calculations, *J. Geophys. Res.*, *89*, 5263–5279.
Kaminski, T., M. Heimann, and R. Giering (1999), A coarse grid three-dimensional inverse model of the atmospheric transport: 1. Adjoint model and Jacobian matrix, *J. Geophys. Res.*, *104*, 18,535–18,553.
Kaplan, J. O. (2001), Wetlands at the Last Glacial Maximum: Distribution and methane emissions, *Geophys. Res. Lett.*, *29*, 6–10.
Kasibhatla, P., A. Arellano, J. A. Logan, P. I. Palmer, and P. Novelli (2002), Top-down estimate of a large source of atmospheric carbon monoxide associated with fuel combustion in Asia, *Geophys. Res. Lett.*, *29*(19), 1900, doi:10.1029/2002GL015581.
Langenfelds, R. L., R. J. Francey, B. C. Pak, L. P. Steele, J. Lloyd, C. M. Trudinger, and C. E. Allison (2002), Interannual growth rate variations of atmospheric CO_2 and it's $\delta^{13}C$, H_2, CH_4, and CO between 1992 and 1999 linked to biomass burning, *Global Biogeochem. Cycles*, *16*, 1048–1070.
Lassey, K. R., D. C. Lowe, and M. R. Manning (2000), The trend in atmospheric methane $\delta^{13}C$ and implications for isotopic constraints on the global methane budget, *Global Biogeochem. Cycles*, *14*, 41–49.
Lelieveld, J., P. J. Crutzen, and F. S. Dentener (1998), Changing concentration, lifetime, and climate forcing of atmospheric methane, *Tellus*, *Ser. B*, *50*, 128–150.
Levine, J. S., W. R. Coffer III, and J. P. Pinto (2000), Biomass burning, in *Atmospheric Methane: Its Role in Global Environment*, edited by M. A. K. Khalil, Springer-Verlag, New York.
Louis, J. F. (1979), A parametric model of vertical eddy fluxes in the atmosphere, *Boundary Layer Meteorol.*, *17*, 187–202.
Lowe, D. C., C. A. M. Brenninkmeijer, G. W. Brailsford, K. Lassey, A. J. Gomez, and E. G. Nisbet (1994), Concentration and ^{13}C records of atmospheric methane in New Zealand and Antarctica: Evidence for changes in methane sources, *J. Geophys. Res.*, *99*, 16,913–16,925.
Masarie, K. A., and P. P. Tans (1995), Extension and integration of atmospheric carbon dioxide data into a globally consistent measurement record, *J. Geophys. Res.*, *100*, 11,593–11,610.
Matthews, E., and I. Fung (1987), Methane emissions from natural wetlands: Global distribution, area, and environmental characteristics of sources, *Global Biogeochem. Cycles*, *1*, 61–86.
McCarthy, M. C., P. Connell, and K. A. Boering (2001), Isotopic fractionation of methane in the stratosphere and its effect on free tropospheric isotopic compositions, *Geophys. Res. Lett.*, *28*, 3657–3660.
Mikaloff Fletcher, S. E., P. P. Tans, L. M. Bruhwiler, J. B. Miller, and M. Heimann (2004), CH_4 sources estimated from atmospheric observations of CH_4 and its $^{13}C/^{12}C$ isotopic ratios: 2. Inverse modeling of CH_4 fluxes from geographical regions, *Global Biogeochem. Cycles*, doi:10.1029/2004GB002224, in press.
Miller, J. B., K. A. Mack, R. Dissly, J. W. C. White, E. J. Dlugokencky, and P. P. Tans (2002), Development of analytical methods and measurements of $^{13}C/^{12}C$ in atmospheric CH_4 from the NOAA/CMDL global air sampling network, *J. Geophys. Res.*, *107*(D13), 4178, doi:10.1029/2001JD000630.
National Oceanic and Atmospheric Administration (2001), GLOBALVIEW-CH_4: Cooperative Atmospheric Data Integration Project- Methane [CD-ROM], report, Clim. Monit. and Diag. Lab., Boulder, Colo. (Also available at ftp.cmdl.noaa.gov, Path: ccg/ch4/GLOBALVIEW)
Novelli, P. C., K. A. Masarie, P. M. Lang, B. D. Hall, R. C. Myers, and J. W. Elkins (2003), Reanalysis of tropospheric CO trends: Effects of the 1997–1998 wildfires, *J. Geophys. Res.*, *108*, 4464–4488.
Olivier, J. G. J., A. F. Bouwman, C. W. M. van der Maas, J. M. Berdowski, C. Veldt, J. P. J. Bloos, A. J. H. Visschedijk, P. J. Zandveld, and J. L. Haverlag (1996), Description of Edgar Version 2.0: A set of global emission inventories of greenhouse gases and ozone-depleting substances for all anthropogenic and most natural sources on a per country basis and on 1×1 grid, report, Natl. Inst. of Public Health and the Environ., Bilthoven, Netherlands.
Page, S. E., F. Siegert, J. O. Rieley, H. D. V. Boehm, A. Jaya, and S. Limin (2002), The amount of carbon released form peat and forest fires in Indonesia during 1997, *Nature*, *420*, 61–65.
Platt, U., and G. Hönninger (2003), The role of halogen species in the troposphere, *Chemosphere*, *52*, 325–338.
Quay, P., J. Stutsman, D. Wilbur, A. Snover, E. Dlugokencky, and T. Brown (1999), The isotopic composition of atmospheric methane, *Global Biogeochem. Cycles*, *13*, 445–461.
Russell, G., and J. Lerner (1981), A new finite-differencing scheme for the tracer transport equation, *J. Appl. Meteorol.*, *20*, 1483–1498.
Sanderson, M. G. (1996), Biomass of termites and their emissions of methane and carbon dioxide: A global database, *Global Biogeochem. Cycles*, *10*, 543–557.
Saueressig, G., J. N. Crowley, P. Bergamaschi, C. Brühl, C. A. M. Brenninkmeijer, and H. Fischer (2001), Carbon 13 and D kinetic isotope effects in the reactions of CH_4 with $O(^1D)$ and OH: New laboratory measurements and their implications for the isotopic composition of stratospheric methane, *J. Geophys. Res.*, *106*, 23,127–23,138.
Spivakovsky, C. M., et al. (2000), Three-dimensional climatological distribution of tropospheric OH: Update and evaluation, *J. Geophys. Res.*, *105*, 8931–8980.
Still, C. J., J. A. Berry, G. J. Collatz, and R. S. DeFries (2003), Global distribution of C_3 and C_4 vegetation: Carbon cycle implications, *Global Biogeochem. Cycles*, *17*(1), 1006, doi:10.1029/2001GB001807.
Sugawara, S., T. Nakazawa, Y. Shirakawa, K. Kawamura, S. Aoki, T. Machida, and H. Honda (1997), Vertical profile of the carbon isotopic ratio of stratospheric methane over Japan, *Geophys. Res. Lett.*, *24*, 2989–2992.
Tans, P. P. (1997), A note on isotopic ratios and the global atmospheric methane budget, *Global. Biogeochem. Cycles*, *11*, 77–81.
Tans, P. P., I. Y. Fung, and T. Takahashi (1990), Observational constraints on the global atmospheric CO_2 budget, *Science*, *247*, 1431–1438.
Tiedke, M. (1989), A comprehensive mass flux scheme for cumulus parameterization in large-scale models, *Mon. Weather Rev.*, *117*, 1779–1800.
Tyler, S. C., P. M. Crill, and G. W. Brailsford (1994), $^{13}C/^{12}C$ fractionation of methane during oxidation in a temperate forested soil, *Geochim. Cosmochim. Acta*, *58*, 1625–1633.
Van der Werf, G. R., J. T. Randerson, G. J. Collatz, L. Giglio, P. S. Kasibhatla, A. F. Arellano, S. C. Olsen, and E. S. Kaisichke (2004), Continental-scale partitioning of fire emissions during the 1997 to 2001 El Niño/La Niña period, *Science*, *303*, 73–76.
Walter, B. (1998), Development of a process-based model to derive methane emissions from natural wetlands for climate studies, Ph.D. thesis, Univ. Hamburg, Germany.
Warwick, N. J., S. Bekki, K. S. Law, E. G. Nisbet, and J. A. Pyle (2002), The impact of meteorology on the interannual growth rate of atmospheric methane, *Geophys. Res. Lett.*, *29*, 1947–1951.
Whiticar, M. (1993), Stable isotopes in global budgets, in *Atmospheric Methane—Sources, Sinks, and Role in Environmental Change*, *NATO ASI Ser.: Global Environ. Change*, vol. 1, edited by M. A. K. Khalil, Springer-Verlag, New York.

L. M. Bruhwiler, J. B. Miller, and P. P. Tans, NOAA CMDL, R/CMDL-1, 325 Broadway, Boulder, CO 80305, USA. (lori.bruhwiler@noaa.gov; john.b.miller@cmdl.noaa.gov; pieter.tans@noaa.gov)
M. Heimann, Max-Planck-Institut für Biogeochemie, Postfach 10064, D-0771 Jena, Germany. (martin.heimann@bgc-jena.mpg.de)
S. E. Mikaloff Fletcher, Department of Atmospheric and Oceanic Sciences, University of California, Los Angeles, 5839 Schlicter Hall, Los Angeles, CA 90024, USA. (fletcher@igpp.ucla.edu)